IEEE Access
Multidisciplinary | Rapid Review | Open Access Journal

Received June 1, 2021, accepted June 18, 2021, date of publication June 25, 2021, date of current version July 2, 2021.

Digital Object Identifier 10.1109/ACCESS.2021.3091738

Techno-Economic Design of a Combined Heat and Power Microgrid for a Remote Community in Newfoundland Canada

HASHEM ELSARAF[1], (Graduate Student Member, IEEE), MOHSIN JAMIL[1], AND BISHWAJEET PANDEY[2], (Senior Member, IEEE)

[1]Department of Electrical and Computer Engineering, Memorial University of Newfoundland, St. John's, NL A1B 3X5, Canada
[2]Birla Institute of Applied Sciences, Bhimtal 263136, India

Corresponding author: Hashem Elsaraf (hasmaelsaraf@mun.ca)

ABSTRACT Around 300 remote communities in Canada rely on diesel for their energy needs, a situation associated with high costs, high emissions, and accessibility problems. Various studies have addressed this problem by proposing renewable energy microgrids, which have a lot of potential due to the abundance and availability of renewable sources. However, there is a lack of studies regarding remote communities in Newfoundland and combined heat and power microgrids. This study chose Cartwright remote community based on consumption and available resources. Both distributed and centralized microgrid components were designed using MS Excel, Polysun, HOMER, and BEOPT. The final system included solar thermal, PV, wind energy, hydroelectric energy and fuel cells for energy generation, and hydrogen as an energy carrier for storage. The solar thermal distributed system reduced the thermal load by 35%. The microgrid reduced diesel consumption by 71% and CO_2 emissions by 9000 tons. Renewable sources provided 100% of the electric load and 63.5% of the thermal load. The microgrid achieved a Levelized cost of -0.0245 $/kWh, which is only possible for combined heat and power systems.

INDEX TERMS Remote communities, microgrids, HOMER, renewable energy generation, energy storage.

I. INTRODUCTION

There are around 300 remote communities in Canada, with over 225,000 residents, which often house vulnerable first nation communities. The overwhelming majority (71%) of these communities have all or part of their electricity and heating demand met by diesel generation, which is polluting and costly since diesel produces 161.3 pounds of CO_2 per million BTU of energy generated and the transportation of the fuel to the farther away locations is more expensive. The transport of diesel is also often hindered due to accessibility problems. The cost of electricity generation in these locations can reach as high as 3.19 $/kWh, whereas the main parts of Canada have an electricity rate as low as 0.07 $/kWh (for Newfoundland (NL), it is 0.123 $/kWh). This leads to a significant percentage of the remote community's budget being allocated for diesel procurement, meaning there is less money available for other uses, which hinders development. NL remote communities also produce 2.6 times more per capita emissions than the Canadian average [1]–[3], [5].

Renewable energy system integration in microgrids (supported by UN sustainability goal 7) can, therefore, significantly reduce electricity generation costs and emissions in such scenarios. These projects also provide an opportunity for partnerships between remote communities and stakeholders, which is an avenue for progress. These communities, however, have varying structures, resources, and priorities and therefore require renewable energy sources (RES) to be specifically tailored for the community [1]–[3].

As a solution, this study will seek to design a microgrid for a Newfoundland community that serves both its electric and thermal energy needs. First, a recent literature survey (2019-2021) regarding this problem will be performed to evaluate the available options. Then a community will be selected based on novelty as well as data and resource availability. Then the appropriate communal and distributed generation and storage elements will be designed, followed by economic analysis.

The associate editor coordinating the review of this manuscript and approving it for publication was Lei Chen.

II. LITERATURE REVIEW

In a 2020 study, the authors presented a case study of the impact of the integration of centralized PV on a diesel-based microgrid's annual performance, emissions, and economics at varying penetration levels and control strategies for a small remote arctic community in northern Canada. They stated that PV and wind systems have a good track record in reducing remote communities' electricity costs. It was found that compared to a diesel price of 1.2 $/L, PV system needs to achieve a price of $5/W or less to be economically competitive [1].

A 2019 study regarding off-grid combined heat and power (CHP) microgrid proposed quantifying renewable energy uncertainties using intraday rolling dispatch strategy with case studies verifying the model's efficacy [2].

A study added to IEEE in 2020 addressed the design of a stand-alone hybrid renewable microgrid for a remote community in Pakistan. The system used PV/wind/diesel and battery hybrid and was analyzed based on levelized cost of energy (LCOE), net present cost (NPC), and emissions. Simulation results showed that PV-wind-battery was the most feasible with an LCOE of 0.311 $/kWh. This study used HOMER Pro software [3].

A stand-alone microgrid that utilizes biomass combustion was investigated for a Canadian aboriginal community in another recent study. The system combined wind, biomass, diesel, and batteries. It was found that biomass power can follow load fluctuations, decrease power produced from diesel, and lower peak load demand on batteries [4]. However, concerns regarding the mass use of biomass have been a concern for several decades. These issues include competition for arable lands, soil disturbances, nutrient depletion, impaired water quality, and production of polluting by-products [18].

In [5], several combinations of energy sources that include renewables, hydrogen, flow batteries, and natural gas were examined for a microgrid for the Sanikluaq remote community in Nunavut. The study used HOMER Pro's optimizer tool to find the optimum combination of energy sources based on location resources and system costs. The results show that a substantial reduction in diesel is plausible for the arctic communities in Canada. More considerable renewable penetration and more diverse generation correlated with more considerable savings and better LCOEs. The final energy mix included solar PV, wind, hydrogen, flow batteries, and natural gas.

In [6], the authors investigated the integration of renewable energy generation with variable speed generators to replace a diesel-only system in remote arctic communities. The study proposed a novel methodology for remote community selection.

In a 2021 study of DC microgrids, the authors addressed problems associated with high renewable penetration, such as adequacy of power supply and voltage provision during the islanded mode. The study developed a probabilistic approach based on Bayesian networks to conduct reliability analysis. The model was verified using Monte Carlo simulations and suggested that different renewables have different impacts on microgrid reliability [7].

In a recent study, uncertainties in designing a microgrid for remote communities were assessed through an analytical network process and experts' surveys. These criteria include institutional support, the possibility of microgrid expansion, and the availability of renewable resources. The results were used in designing a microgrid for a community where it was found that wind and solar are the best technologies coupled with biomass backup gasifiers [8].

In relevant studies regarding CHP microgrids, the ratio of electric energy output to thermal energy output was controlled together with demand-side management to minimize the overall microgrid operational cost [10]. A microgrid that includes an electric vehicle (EV) station, CHP cogeneration, water storage tank, and other systems was designed where EV batteries (managed through a proposed algorithm) were used as energy storage to reduce operational costs [11]. However, while EVs are promising as energy storage systems in microgrids they suffer from economic constraints that limit their feasibility [14]. This makes them potentially incompatible with remote community microgrids.

Regarding solar thermal energy in Canada, a study found that coupling solar thermal collectors with heat pump water heaters can fully offset the cooling effect of said heaters and decrease the space heating load by up to 3% and space cooling load by up to 15% [15]. In a cradle to grave lifecycle analysis, it was found that Canadian homes that utilize solar thermal have 70% lower emissions than conventional homes [13]. However, the authors of [12] highlight that the large mismatch between solar thermal supply and demand is an ongoing issue that can be reduced by the inclusion of both thermal energy storage and an effective control strategy.

A few recent studies addressed hydrogen electrolysis as a form of storage in renewable microgrids. Compared with a diesel reference case, the hydrogen storage microgrid was able to provide 66%-99% carbon emission reduction but at 30%-100% increased cost. The hydrogen fuel was used to power fuel cell vehicles, busses, and trucks as well as utility electricity generation [16]. While in another study, resilience against extreme events was improved via hydrogen-based CHP microgrids by lowering the risk of load interruption [17]. A third study highlighted the importance of hydrogen in emerging smart cities as it incurs profits for consumers through energy trading and increases energy resilience [19].

Lastly, only one recent study was found that addressed a microgrid design for a remote community in Newfoundland. In this study, a pumped hydro storage system was compared against a battery-based storage hybrid system in technical, environmental, and economic aspects using HOMER. The results show an LCOE that is 62% lower than the diesel-only base case. This study developed a zero-emissions system that did not require any diesel or natural gas generators [9].

There are, however, a few noteworthy critiques of the previous study. For example, the studied community (Grey River) is too small with an unremarkable diesel consumption

TABLE 1. List of diesel-run remote communities in Newfoundland and their properties.

Designated place	D#	Cap.	AEE.	NP.	AFC.	Trans.	Pop.	H#	Area	WS.	WE.	GHI	H
Francois	3	635	657.2	204	193,15	Ship	89	54	5.09	7.48	519.5	1147	81.6
Grey River	3	522	499.4	180	161.32	Ship	104	57	2.44	6.98	453.62	1081	81.6
Mccallum	3	446	462.9	133	144073	Ship	73	48	1.82	7.14	465.12	1118	-
St. Brendan's	3	712	974.3	280	281.24	Ship	145	137	10.14	8.73	646.62	1123	-
Charlottetown	5	3405	5033	1421	1,479,138	-	290	128	30.53	8.38	509	1111	13.8
Norman Bay	3	160	230	50	79,66	Ship	369	242	36,629	8.05	480.38	1138	-
Mary's Harbour	4	2615	4253	928	1,350,737	Truck	65	37	6.19	7.94	464.75	1143	74.6
Port Hope Simpson	4	2325	3420	723	1,046,011	Truck	412	176	32.52	8.48	521.62	1119	64.8
St. Lewis	3	1020	1580	378	436,994	Truck	194	89	9.25	8.3	524.50	1087	74.6
Black Tickle	3	1005	1162	287	324,902	Ship	150	82	9.43	9.04	710.75	1066	-
Cartwright	4	2220	4645	1037	1,304,991	Truck	427	221	3.27	8.64	625.25	1107	300
Paradise River	3	148	220.4	65	88,246	Truck	369	242	36,629	7.38	418.38	1082	300

D# = Number of diesel generators, Cap.= total capacity of diesel generator (kW). AEE. = Annual electric energy generation (MWh), NP. = Net Peak (kW), AFC. = Annual fuel consumption (L), Trans.= Mode of Fuel transportation, Pop.= Population (2016), H# = Number of houses, Area = Land area (km^2), WS. = Annual mean wind speed (m/s) for 30m hub height, H= nearby hydro resource mean flow rate (m^3/sec), GHI= Global horizontal irradiance (kWh/m^2), WE. = Annual mean wind energy (W/m

(and therefore emissions). The use of pumped hydro storage is too location-specific, limiting the generalisability of the study results. Load profiling was too simplistic, whereas a more thorough methodology such as BEOPT could be utilized. The study did not consider the thermal load (which can be 4 to 5 times the electric load size). The study also did not consider hydrogen electrolysis as a form of storage that (if widely applied) can enable remote communities to engage in energy trading with each other and with mainland areas that would have economic and developmental implications and allow for combined heat and power generation.

Therefore, this study will seek to choose an appropriate remote community in NL, design a multi-faceted system that includes hydrogen storage, conduct thorough load profiling using BEOPT, consider the thermal load by designing a CHP microgrid, and include solar thermal as one of the systems.

In short, the main contribution of this research can be summarised as:

1. In past, researchers have used HOMER to design microgrids, but they did not include a solar thermal system since HOMER can't design that. In this research, solar thermal system was included using MS Excel and Polysun.
2. Authors are not aware of any recent study (2019-2021) that addressed a CHP microgrid design in a remote community in Newfoundland. The heating load in Canada is 4-5 times the size of the electric load and therefore a major contributor to emissions should be considered.
3. Additionally, the contribution of this paper involves boarder load profile and generic location for storage technology. This study involves a community with high consumption/emissions, load profiling using BEOPT, and choosing hydrogen electrolysis as storage.

III. COMMUNITY SELECTION

Thirteen remote NL communities use only diesel for their energy generation, as presented in Table 1. This table was created by combining six different sources, including the Canadian wind atlas, global solar atlas, Canada's water office data, and Canadian census data. As can be seen, the eastern community of Cartwright (53° 42' 28" N, 57° 0' 58" W) stands out for having the highest hydro resource, very high diesel consumption (and therefore emissions), very high wind energy, and the highest population making it a priority when it comes to designing a renewable energy microgrid. Figure 1 shows a map of communities in NL and their energy sources.

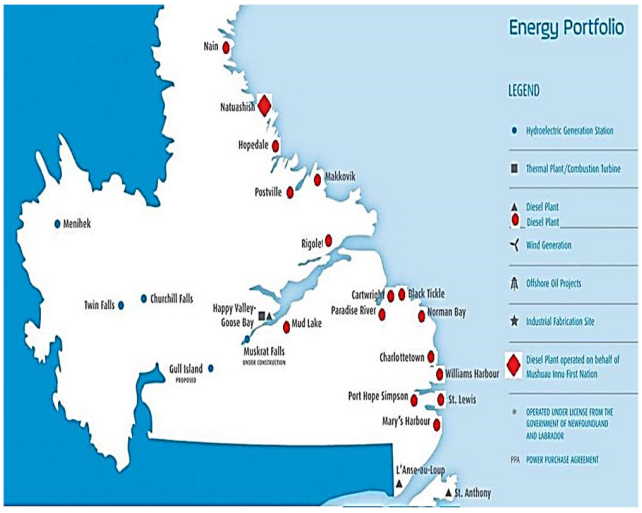

FIGURE 1. Map of NL communities and their associated energy sources.

Cartwright is a remote community on the eastern side of Newfoundland's province with a land area of 3.27 km^2. It had 427 residents in 2016, which is a 15.3% decrease from 2011 demographics. The community uses four diesel generators with a combined capacity of 2220 kW, which produces 4.65 GWh of electricity annually. The community is made up of 221 dwellings, 188 of which are private dwellings currently occupied. The average number of rooms per dwelling is around six rooms which allow for the simulation of the load using BEOPT by surveying a 6-room older house in St. John's. This yields both electrical and thermal hourly loads,

which allow for the design of a hybrid power and heat microgrid with both centralized and distributed elements. Other significant loads include the fish plant, the hotel, the hospital, the school, the marine center, the coast guard stations, and the airstrip. For this study's purposes, all built dwellings will be considered occupied to size a system compatible with future load growth. Results show that the residential sector represents 64.3% of the community's electricity consumption, with the other significant loads consuming the remaining 35.7%. This allows the modeling of the non-residential electrical and thermal loads as multiples of residential loads.

IV. METHODOLOGY

In this section a discussion of the selected software will be conducted, followed by solar thermal design mathematical modeling, followed by a review of the renewable energy resources of the selected location and a brief explanation of component selection.

A. SOFTWARE UTILIZED

1) HOMER

HOMER is short for Hybrid Optimization Model for Multiple Energy Resources. It is a toolbox used for microgrid design for remote communities. It was developed by the US National Renewable Energy Laboratory (NREL) to help with the optimal design of both grid-tied and off-grid microgrids by offering simulations of the long-term performance of such systems. It has become the global standard for microgrid/hybrid energy system design. An essential advantage of HOMER is the simulation of various alternatives and combinations of energy generation and storage such as PV modules, batteries, wind turbines, biomass generators, fuel cells, hydrogen storage, and small hydro.

Inputs to HOMER include location, resources, generation components specification and cost, loads, energy storage specifications, and grid values and policies. This software application is used to design and evaluate technically and financially the options for off-grid and on-grid power systems for stand-alone remote applications. It allows the user to consider many technology options to account for energy resource availability and other variables.

HOMER simulation operates via energy balance calculations for each interval (time step) of the year (usually per hour). It compares the energy generated in that interval with the electric and thermal demand of that interval. Thereby calculating the energy flow to and from each system component. HOMER also decides whether or not batteries need to be charged/discharged or fuel generators need to be turned on. One limitation of HOMER, however, is its inability to simulate solar thermal systems. A flowchart of the steps involved in the design is shown in figure 2.

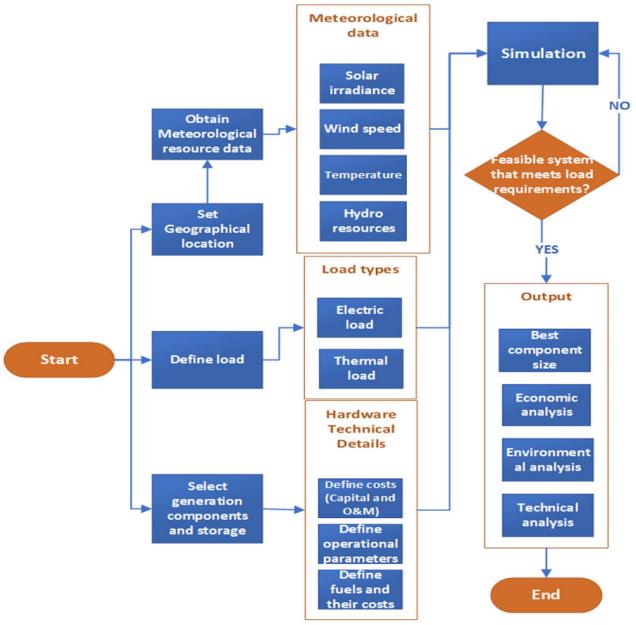

FIGURE 2. HOMER simulation design flowchart.

2) BEOPT

BEOPT is short for Building Energy Optimization Tool. It is a software developed by NREL, affiliated with the US department of energy (DOE), often used to simulate the electrical and thermal loads for the studied dwellings with a high degree of accuracy. It can be used to identify the most cost-optimal efficiency designs and their resulting energy savings for new constructions or to design retrofits. BEOPT provides detailed results based on house characteristics, size, architecture, occupancy, location, and utility rates. It utilizes the US DOE-developed simulation engine EnergyPlus. A flowchart of the steps involved in the design is shown in figure 3.

BEOPT is an accurate and useful tool that has been involved in various studies. In recent studies BEOPT was utilized in the design of low-cost energy efficiency measures, hybrid residential systems for off-grid homes, net-zero energy buildings, hybrid PV-biomass distributed generation for rural housing in Morocco, and evaluation of the best paths to net-zero energy for geothermal heat pump HVAC plus solar systems across 12 U.S. climate zones to determine the optimal configuration for each zone [22]–[25].

3) POLYSUN

Polysun was developed in 1992 by the Institute for Solar Technology (SPF) at the University of Applied Sciences in Rapperswil, Switzerland. The software includes more than 1000 built-in templates that are based on actual/practical project layouts. The program provides economic and GHG emission analysis.

Recent studies have used Polysun such as a hybrid grid-connected PVT system used for electricity generation, space heating, and water heating for a single-family house [20].

However, in a different study, an hourly model based on energy balance equations was used to simulate a domestic hot water (DHW) solar thermal system and compared

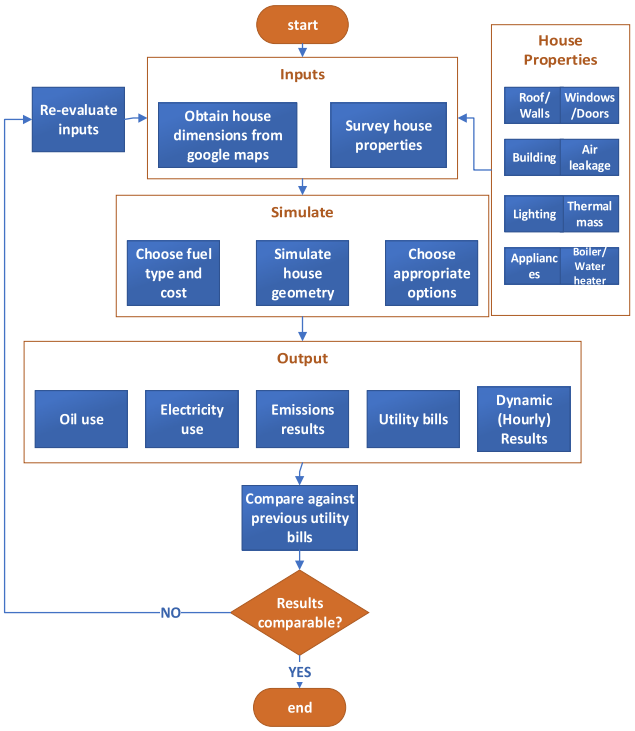

FIGURE 3. BEOPT simulation design flowchart.

against Polysun results. While the comparison showed similar results, Polysun's use of auxiliary heating was deemed by the authors as being either undersized or oversized depending on the control layer (89.5% error). This was seen as being due to Polysun's usage of a temperature stratification model for the storage tank [21].

B. MATHEMATICAL MODELING

1) SOLAR THERMAL

Hottel–Whillier–Bliss (HWB) equation (equation 2) for flat plate collectors can be used to calculate the proper amount of energy output from the collector and the collector efficiency. First, efficiency can be defined as the ratio of useful energy to the input of solar energy (equation 1) such that:

$$\eta_c = \frac{Q_{useful}}{Q_{in}} = \frac{A_c[I_T\tau\alpha - U_L(T_{avg} - T_a)]}{I_T A_c} = \tau\alpha - U_L\frac{T_{avg} - T_a}{I_T} \quad (1)$$

Replacing average collector temperature T_{avg} with inlet fluid temperature T_{in} yields

$$\eta_c = F_R\tau\alpha - F_R U_L\frac{T_{in} - T_a}{I_T} \quad (2)$$

where: η_c = Collector efficiency (unitless), F_R = collector heat-removal factor (unitless), τ = cover glass transmissivity (unitless), α = absorber plate absorptivity (unitless), U_L = Overall conductance, I_T = irradiance (W/m^2) and A_c = total collector area (m^2), $F_R\tau\alpha$ = intercept (unitless) and $F_R U_L$ = slope (W/m^2.°C), T_{in} is the fluid inlet temperature (°C), and T_a is the ambient temperature (°C)

Q_{useful} can then be calculated using equation 3:

$$Q_{useful} = \eta_c * I_T * A_c \quad (3)$$

Due to the 1st law of thermodynamics, Quseful can also be given by the sensible heat equation as equation 4

$$Quseful = \dot{m}c_p\,(T_{out} - T_{in}) \quad (4)$$

where: $\dot{m}$ = mass flow rate of the fluid., c_p = Specific heat of HTF (4.186 kJ/kg °C for water)., $T_{out} - T_{in}$ = Temperature difference of fluid at inlet and outlet of the collector.

There is room for energy storage contribution in solar thermal systems since the unmet load and excess energy parameters without it are relatively high. In this section, sensible heat unstratified water storage is examined. Equation 5, used to calculate the storage temperature, the energy delivered by the storage as well as the losses, is:

$$T_s^+ = T_s + \frac{\Delta t}{mc_p} * (Q_u - L_s - (UA)\,(T_s - T_b)) \quad (5)$$

where: T_s^+ is the storage temperature at the end of the period (1 hour) (°C), T_s is the storage temperature at the beginning of the storage period (1 hour) (°C), Δt is the period which in this case is 1 hour, m is the mass of the storage water (kg), c_p is the specific heat of the storage medium (4190 J/kg °C), Q_u is the rate of addition of energy to storage (collector output) (J), L_s is the rate of removal of energy from storage (load) (J), UA is the product of heat loss coefficient and area, T_b is the ambient temperature of the basement where the storage is placed.

From equation 5, the term inside the bracket can be used to describe the tank losses such that equation 6 is given by:

$$Tank\ losses = (Q_u - L_s - (UA)\,(T_s - T_b)) \quad (6)$$

The initial temperature was assumed as 60 °C, but it could be any value as it has a negligible impact on overall results. UA product is assumed at 11.1 W/°C. Two nested conditions are used to limit the water temperature to between 5 °C, and 95 °C since the phase change temperature of water limits its application. Practically this means that, for example, if the temperature of the water in the tank reaches 95 °C, then no more energy should be added to it as this would lead to evaporation. So, this scenario's surplus energy would have to be utilized differently (such as fed to a dump load). The last term in the brackets $(Q_u - L_s - (UA)\,(T_s - T_b))$ can be used to calculate tank losses. For this study, a standard 60-gallon water tank will be assumed.

2) SOLAR PV

HOMER calculates PV energy output using equation (7) which relates the rated PV panel capacity with the derating factor, solar radiation, and temperature.

$$P_{PV} = Y_{PV} * f_{PV} * \left(\frac{G_T}{G_{T,STC}}\right) * [1 + \alpha_p\,(T_c - T_{c,STC})] \quad (7)$$

where: P_{PV} is the output of the PV array (kW), Y_{PV} is the rated capacity of the PV array (kW), f_{PV} is the derating factor, G_T solar radiation incident on the PV array in kW/m^2 while $G_{T,STC}$ is the standard test condition (STC) incident radiation which is 1 kW/m^2. α_p is the temperature coefficient of power which describes the % decrease in power per °C increase in temperature. T_c is the PV's cell temperature (°C) while $T_{c,STC}$ is the PV cell's temperature under STC (25 °C).

3) WIND ENERGY

HOMER calculates the output power of wind turbine in each time interval by first calculating the wind speed at the selected hub height, then output power at standard air density, then air density height adjustment is made and power output is recalculated.

Hub height wind speed is calculated using equation (8)

$$V_{hub} = V_{anem} * \left(\frac{Z_{hub}}{Z_{anem}}\right)^{\alpha} \tag{8}$$

where: V_{hub} is the wind turbine hub height wind speed (m/s), V_{anem} is the anemometer wind speed (m/s) and Z_{hub} and Z_{anem} are the wind turbine hub height (m) sand anemometer height (m) respectively.

The wind turbine's power curve is then used to calculate the output power under standard conditions then air density correction is performed using equation (9)

$$P_{actual} = P_{standard} * \left(\frac{\rho}{\rho_o}\right) \tag{9}$$

where: P_{actual} is the actual wind turbine output after air density correction in kW. $P_{standard}$ is the wind turbine output under standard temperature and pressure in kW. ρ_o is the standard air density (1.225 kg/m^3) while ρ is the actual air density in kg/m^3.

4) HYDROPOWER

HOMER uses equation (10) to relate the power output of the hydro turbine to the turbine's efficiency, water density, head, and flow rate

$$P_{hyd} = (\mu_{hyd} * \rho_{water} * g * h_{net} * Q_{turbine}) * \frac{1kW}{1000W} \tag{10}$$

where: P_{hyd} is the out power of the turbine in kW, μ_{hyd} is the turbine's efficiency (%), ρ_{water} is the standard density of water (1000 kg/m^3), g is the gravitational acceleration (9.8 m/s^2), h_{net} is the effective head and $Q_{turbine}$ is the turbine's design flow rate (m^3/sec).

5) FUEL CELL

Generally, a generator consumes fuel to produce electricity and heat. HOMER generator module can simulate a variety of generator types such as internal combustion engines and fuel cells. Electrolyzed hydrogen from a hydrogen tank is a specialized fuel that the user can select. Important characteristics of a generator are its minimum and maximum electrical output, the fuel it consumes, the fuel curve, and its expected operating hours. HOMER uses equation (11) to calculate the generator's fuel consumption while assuming the fuel curve is a straight line with a y-intercept.

$$F = F_o * Y_{gen} + F_1 * P_{gen} \tag{11}$$

where: F_o is the fuel curve's y-intercept, F_1 is the curve's slope, Y_{gen} is the generator's rated capacity in kW and P_{gen} is the generator's electrical power output in kW. The units of F, F_o and F_1 depend on the unit the fuel is measured in. If the fuel is measured in liters F is in L/h while F_o and F_1 are in L/h*kW.

HOMER assumes that the generator converts all of the fuel's energy into electricity and waste heat. For systems that utilize heat (such as fuel cells), a heat recovery ratio is specified which is the fraction of waste heat that can be secured to serve the thermal load. HOMER decides whether the generator should be operated based on system needs and relative cost. When the generator is switched on HOMER decides at what power level it should be operated.

Based on multiple cost factors HOMER then calculates the generator's fixed and marginal cost of energy using equations (12) and (13). Where the fixed cost is the per hour cost of running the generator without generation while the marginal cost is the additional cost incurred per kWh of electricity produced

$$c_{gen,fixed} = c_{o\&m} * \frac{C_{rep}}{R_{gen}} + F_o Y_{gen} c_{eff} \tag{12}$$

where: $c_{gen,fixed}$ is the generator's fixed cost, $c_{o\&m}$ is the operations and maintenance (O&M) cost in $/hr, c_{rep} is the replacement cost, R_{gen} is the lifetime of the generator in hours, F_o is the fuel curve y-intercept, Y_{gen} is the generator capacity in kW and c_{eff} is the effective price of fuel including emission-related cost penalties in $/L.

$$c_{gen,mar} = F_1 * c_{eff} \tag{13}$$

where: $c_{gen,mar}$ is the generator's marginal cost, F_1 is the slope of the fuel curve in L/hr*kW, c_{eff} is the effective price of fuel including emission-related cost penalties in $/L.

C. LOCATION RESOURCES

In this section, the three primary renewable resources of the design location, namely, wind, solar and hydro, will be briefly discussed.

1) SOLAR RESOURCES

The solar resource for Cartwright is summarized in Table 2 and figures 4 and 5. They illustrate that the global horizontal irradiance is 10.7% higher than the STC of 1000 kWh/m^2, which is noteworthy for a location in Canada and supported by literature that proposed PV-diesel hybrid systems. The location has a PV potential of around 1200 kWh of energy for every kWp of installed PV. The average temperature is also low, meaning any performance degradation due to increased temperature is unlikely. A maximum average temperature of 14.2 °C occurs in July, which is also lower than the selected

TABLE 2. Solar characteristics for the design location.

Variable	Value	Unit
Direct normal irradiation (DNI)	1195	kWh/m^2
Global horizontal irradiation (GHI)	1107	kWh/m^2
Diffuse horizontal irradiation (DIF)	529	kWh/m^2
Global tilted irradiation at the optimum angle	4123	kWh/m^2
Optimum azimuth angle	180	°
The optimum tilt of PV modules	46	°
Average air temperature	0.6	°C

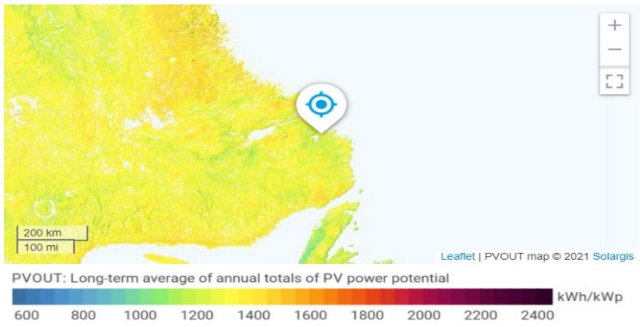

FIGURE 4. PV Output (kWh/kWp) at Cartwright, NL.

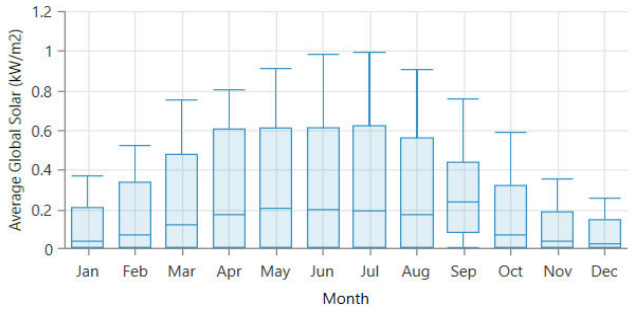

FIGURE 5. Average monthly solar irradiance at Cartwright, NL.

TABLE 3. Wind characteristics and turbine output estimate for the design location for 80m hub height.

Period	MWS.	MWE.	WSP.	WSP.	PO.	EO.
Annual	9.49	820.62	1.99	10.71	2131	18680
Winter	10.85	1186.5	2.06	12.25	2412	5286
Spring	8.79	711.38	1.83	9.89	1931	4232
Summer	7.02	368.81	1.80	7.89	1468	3217
Fall	9.34	788.62	1.97	10.54	2094	4589

MWS.= Mean wind speed (m/s), MWE.= Mean wind energy (W/m^2), WSP.= Weibull shape parameter k, WSP.= Weibull scale parameter c (m/s). PO. & EO. = Power (kW) and Energy (MWh) Outputs of 1 Siemens SWT 3.6 Wind turbine at the design location.

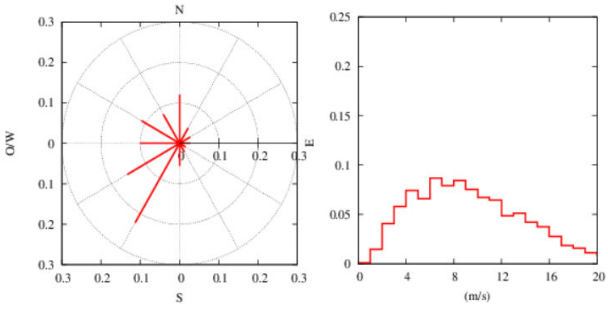

FIGURE 6. a) Wind rose showing wind direction, b) Wind speed histogram at 80m hub height at Cartwright, NL.

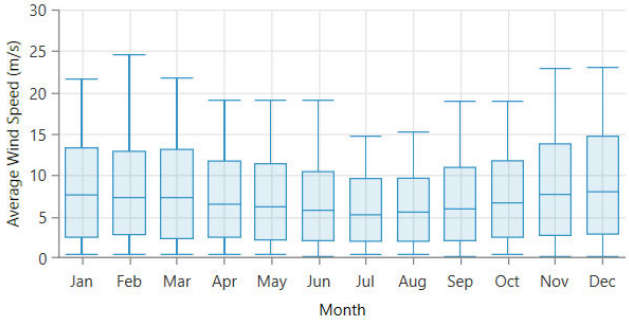

FIGURE 7. Wind speed monthly average at Cartwright, NL.

module's nominal operating cell temperature. According to the solar atlas, the PV panel's optimum tilt angle for the design location is 46°C south-facing. Figure 5 shows the average monthly solar irradiance. From it, we observe irradiance peaking in July and reaching its lowest in December.

2) WIND RESOURCES

Table 3, figure 6, and figure 7 show the characteristics of the wind resource at Cartwright. At 80m hub height, the average wind speed is 9.49 m/s which, if utilized by the wind turbine (WT) selected for this study (Siemens SWT 3.6), would result in an annual energy output of 18.7 GWh. From the wind rose, we observe that the wind is mostly in the Southwestern direction. From the histogram, we observe that wind speeds are mostly between 7 and 9 m/s, and from figure 7, we note that the average wind speeds are mostly the same for every month; however, maximum wind speeds peak in February and dip in the summer, which mimics the behavior of the thermal load making the wind resource very important for a CHP microgrid in Canada.

3) HYDRO RESOURCES

Eagle River, which feeds into Sandwich bay, is the primary hydro resource in the area. It is located 30 km southwest of Cartwright. 2019 water discharge data obtained from Canada's water office (figure 8) shows a minimum discharge of 16 m^3/sec during icy conditions, a maximum discharge of 1,630 m^3/sec, and an overall discharge mean of 300 m^3/sec, i.e., 300,000 L/sec. Using Google Earth Pro (figure 9), a path can be created along the last 13.3 km of the river to find its elevation. The results show an elevation drop of 20m between kilometer 6.3 and kilometer 8.9. This short distance can therefore be used to establish the head for the hydro system.

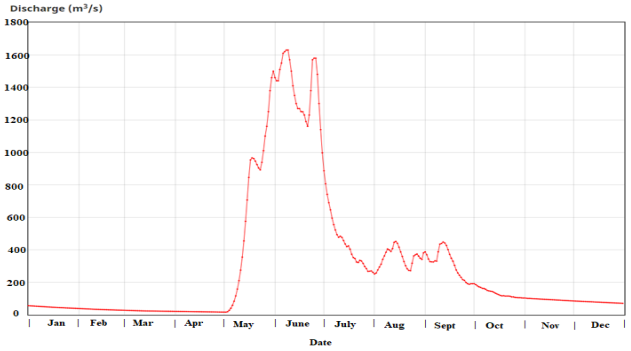

FIGURE 8. Annual water discharge rate at eagle river in m^3/s for 2019.

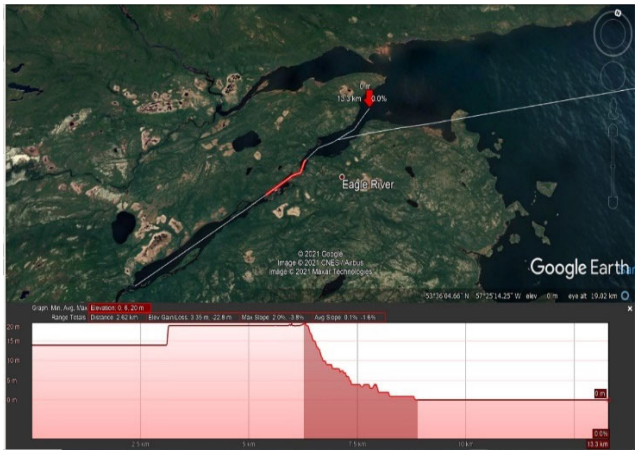

FIGURE 9. Google earth pro analysis of eagle river showing elevation profile and location selected for hydro project.

TABLE 4. AE-21 solar thermal collector characteristic.

Turbine characteristics	Value
Collector type	Glazed Flat Plate
Area	1.932 m^2
Fluid capacity	2.7 L
Glazing	One layer glass
Absorber	Copper tubes and fins
Coating	Selective
Transmissivity/absorptivity	0.9/0.96
Thermal performance	2.68 kWh/m^2
$F_R\tau\alpha$ (optical efficiency)	0.749
$F_R U_L$ (losses coefficient)	-6.159 W/m^2°C

D. SYSTEM COMPONENTS

1) SOLAR THERMAL MODULE

This study's solar thermal collector is AE-21 from Alternate Energy Technology, a widely used collector in the literature [26]. Its relevant properties are shown in Table 4.

2) SOLAR PV MODULE

By considering all PV modules available on the market as provided by Go Solar California (22,000 modules), the best module can be selected based on fill factor (0.72-0.79), efficiency (19.5-22%), degradation rate (88% or higher after 25 years), power density, and module price.

TABLE 5. LG365Q1C-A5 PV module characteristic.

Tech.	Po.	TC.	NOCT	Eff.	DF.	LT.
Monocrystalline	365 W	-0.32 %/°C	45.7 °C	21.1 %	88.4 %	25 years

Tech.= technology, Po.= Power, TC.= temperature coefficient, NOCT= nominal operating cell temperature, Eff. = efficiency, DF. = derating factor, LT.= lifetime.

Building-integrated modules and modules that produce AC power (microinverters), as well as power degradation due to temperature, were disregarded while fill factor and efficiency were prioritized. While CSUN275-60P had a superior fill factor, the final selection was between LG365Q1C-A5 and SPR-X22-360-COM due to efficiency and price. The comparison showed that both modules are high in efficiency and fill factor with the LG module being cheaper while the SunPower module has a better degradation rate. Consequently, LG365Q1C-A5 was preferred, and the main characteristics of the PV panel are shown in Table 5. Sizes ranging from 0 to 12728 kW were considered.

3) INVERTER

The government of California also offers an updated list of all available inverter modules in the market. By sorting and filtering the modules based on the type of inverter, power, price, and compatibility with the current application, SC-2200-Us inverter from SMA was selected. Sizes ranging from 2200 to 11000 kW were considered. The main characteristics of the inverter are shown in Table 6.

TABLE 6. SC-2200-Us inverter characteristic.

Turbine characteristics	Value
Power	2200 kW
Manufacturer	SMA.
Minimum voltage	570 V
Maximum voltage	950 V
Cost	0.18/Watt
Lifetime	15 years
Efficiency	98.6%

4) WIND TURBINE

The selected wind turbine is Siemens SWT 3.6. It was the most profitable based on a 36 parametric study of five different wind turbines (GE-2.5 XL, Vestas 164, Enercon E-126, GE 1.5s, and Siemens SWT 3.6 120) at four locations in NL (Portugal cove, Bonavista, Grand Banks, and Saint Brid's) at different hub heights. The turbines were selected based on a review of the most prominent wind farms inside and outside of Canada. The study included both area and economic considerations where SWT 3.6 was the most economical and E-126 the most area efficient. Since Canada has no shortage of utilizable areas, SWT 3.6 is the preferred option. Table 7 and figure 10 show the turbine's main characteristics. Sizes ranging from 1 to 5 turbines were considered.

TABLE 7. Siemens SWT 3.6 120 wind turbine characteristics.

Turbine characteristics	Value
Rated power	3.6 MW
Cut-in wind speed	3.5 m/s
Cut-out wind speed	25.0 m/s
Rated wind speed	12 m/s
Rotor diameter	120 m
Number of blades	3
Type of generator	Asynchronous generator
Tip speed	104 m/s
Voltage	690 V
Grid frequency	50.0 Hz

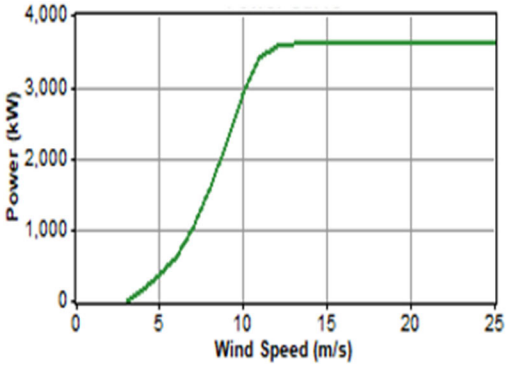

FIGURE 10. The power curve of Siemens SWT 3.6 120 wind turbine.

5) HYDROELECTRIC TURBINE

The hydro turbine considered for this study is the same as the one used in [9]. It is a 100-kW turbine with a 500 L/s design flow rate, 25 years lifetime, 15% pipe losses, 80% efficiency, and 20m available head. The turbine was selected since it is a micro-hydro turbine that runs off continuously flowing water and requires no dams or reservoirs. The size of the turbine and design flow rate was deemed as appropriate for the design location's head, and discharge rate.

6) FUEL CELL

Fuel cells can be regarded as a type of battery that generates electricity and heat from a fuel (mostly hydrogen) and an oxidant (air or oxygen). To model the hydrogen system, a fuel cell, an electrolyzer, and a hydrogen tank are needed. The Fuel cell used was obtained from [5]. It uses stored hydrogen as fuel, has a capacity of 250 kW, a minimum load ratio of 0%, a lifetime of 50,000 hours, CHP recovery ratio of 60%. Sizes ranging from 250 to 2500 kW were considered,

7) ELECTROLYZER/HYDROGEN TANK

The Electrolyzer produces hydrogen by water electrolysis using excess renewable electricity from the microgrid while the tank stores the hydrogen at high pressure for later use. The Electrolyzer (obtained from [5]) has a capacity of 330 kW. It is connected to the DC bus to convert excess electricity to hydrogen. It has an efficiency of 85% and a lifetime of 15 years. Sizes ranging from 330 kW to 1320 kW were considered. Hydrogen tank sizes ranging from 200 kg to 2000 kg were considered.

TABLE 8. Microgrid system component size and price.

System component	Size	Capital ($)	O&M
PV	365 W	450	4.65 ($/yr)
Converter	2200 kW	501,952	0
Wind turbine	3600 kW	3,171,000	95,130 ($/yr)
Solar thermal	48 collectors*	35,760	0
Hydro	100 kW	170,000	50,000 ($/yr)
Fuel cell	250 kW	1,685,810	20 ($/hr)
Electrolyzer	330 kW	1,279,222	194 ($/yr)
Hydrogen tank	200 kg	250,000	12,400 ($/yr)
Electric heater	36 kW*	964	0

* Installed capacity per dwelling as the component is distributed generation.
Note all prices are in Canadian dollars.

8) ELECTRIC HEATER

Based on a survey of modern electric heaters, a heater is chosen, which has 36 kW capacity and a 20-year lifetime. 344 such heaters are to be installed, one on each dwelling, to serve part of the thermal load with excess energy from the renewable system, which lowers the boilers' diesel consumption. Energy star electric water heaters with heat pump technology were also considered due to higher energy factors (greater than 3) to be placed in the heated basement near the boiler. These heaters are so efficient at removing ambient heat that they can actually be used for space cooling in the summer. However, they cost more, have more requirements for efficient operation, and cannot be simulated in HOMER.

9) COMPONENT PRICE

The following table shows the capital and operations and maintenance (O&M) costs of all selected system components.

V. RESULTS AND DISCUSSION

In this section, the results from the load simulation using BEOPT, solar thermal design using the presented methodology and using Polysun and the microgrid design using HOMER will be discussed and analyzed.

A. HOUSE SIMULATION

In this section, the load is simulated by first surveying the house owner to find the relevant properties (Table 9). Physical dimensions of the house are obtained from Google Earth Pro and simulated in BEOPT as shown in figure 11. The results show the house's electric and thermal loads and the associated diesel consumption and what the house pays each year on energy, and the resulting annual emissions as shown in figure 12 and Table 10. Important house properties include the thermal mass, insulation, water, and space heating technology's type and efficiency, air leakage, appliances, and type of lighting. House dimensions, number of rooms, occupancy, and neighbor offsets are also essential inputs. The diesel and electricity prices were also inputted as 2.391 $/L and 12.2 ¢/kWh, respectively.

TABLE 9. House properties survey result.

Option	Value	Option	Value
Wood Stud	R-13 fiberglass	Central AC.	None
Wall Sheathing	R-10 XPS	Boiler	Oil 80%
Exterior Finish	Vinyl, light	Ducts	15% Leak.
Unfin. Attic	R-30 fiberglass	Ceiling Fan	None
Roof Material	Asphalt dark	Dehumidifier	Stand-alone
Radiant Barrier	None	Cooling S.P.	None
Finished Base.	Whl. Wall R-10	Humidity S.P.	45%
Carpet	0%	Heating S.P.	71F sb. 65F
Floor Mass	Wood Surface	Cooling S.P.	None
Ext. Wall Mass	5/8 Drywall	Water Heater	50-gal oil
Partition Wall	None	Solar Water h.	None
Ceiling Mass	5/8-inch DW.	Refrigerator	Top freezer
Windows	Dbl. non-metal	Clothes Wsh.	EnergyStar
Door Area	20 ft^2	Clothes Dryer	Electric
Doors	Wood	Extra fridge.	Top Freezer
Eaves	3 ft	Freezer	Chest EF24
Overhangs	None	PV system	None
Mechanical Vent.	None	Natural vent.	Three days/week

S.P.= setpoint, sb. = setback, Unfin.= unfinished, Base. = basement, h. = heater, Whl.= whole, Dbl. = double, Wsh.= Washer, D.W. = Drywall.

FIGURE 11. a) Design house dimensions and offsets from Google earth pro, b) House simulation in BEOPT.

TABLE 10. Load information (single dwelling).

Parameter	Value
Electricity consumption	13,505 kWh/year
Heating consumption	65,805 kWh/year
Utility bills	16,309 CAD/year
Diesel use	1615 gal/year
Area	344.12 sqm
Emissions	29.4 tonnes/year

B. SOLAR THERMAL RESULTS

Using the equations provided in the methodology, a solar thermal system with a 60-gallon storage tank is designed using MS Excel. Its output is subtracted from the thermal load before entering the load into HOMER. The system is designed as the distributed generation that is installed on each dwelling in the community. The solar thermal system is sized

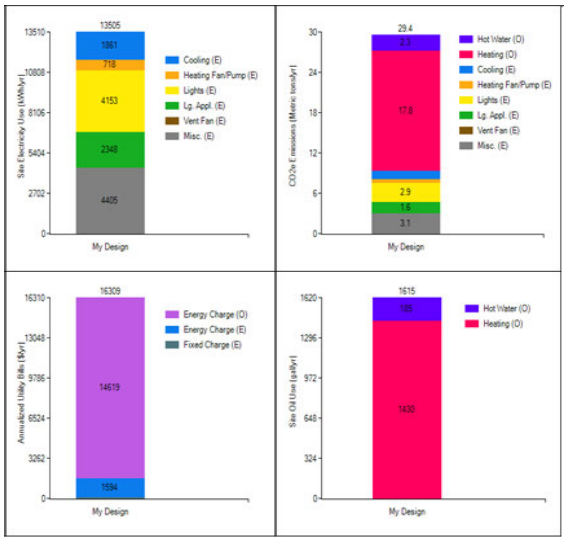

FIGURE 12. BEOPT load simulation results.

so that, assuming no mismatch between supply and demand (i.e., no excess or deficit energy), the system can generate all of the thermal load required by the house. Nevertheless, upon considering the mismatch between supply and demand, the actual load served (also known as the solar fraction) is much lower than 100%. The solar fraction value is slightly improved through the inclusion of thermal energy storage in the form of a 60-gallon water tank installed in each house. The solar thermal system's cost is later added to the electric water heater's cost in HOMER to include it in the financial analysis. The results are analyzed for a single house which is later on scaled up for the whole community.

The inputs to the system include hourly irradiance and ambient temperature (which were obtained from Canada's meteorological website and HOMER) as well as collector's intercept and slope (obtained from AE-21 datasheet). The temperature of the water at the inlet of the collector is assumed as 15 °C. It is found that the number of collectors needed to serve the thermal load is 48 collectors, which occupy 93 m^2 of the 159 m^2 of available rooftop area.

First, efficiency is calculated and then used to calculate the energy output (shown in figure 13 and Table 11). Then the hourly thermal load is subtracted from the hourly energy output to determine energy surplus/deficit. It is found that without energy storage, the 48 collectors can only serve 26% of the load. This is due to solar thermal output peaking in the summer while the thermal load peaks in winter as shown in figure 14.

To understand the effect of collector size on the output, a sweep of sizes ranging from 1 to 48 collectors is done. The parameters investigated are excess energy, unmet load, gallons of oil needed to serve the load after the collector array is installed, the annual sum paid on oil, system payback period, gallons of oil offset per 100 dollars invested, and

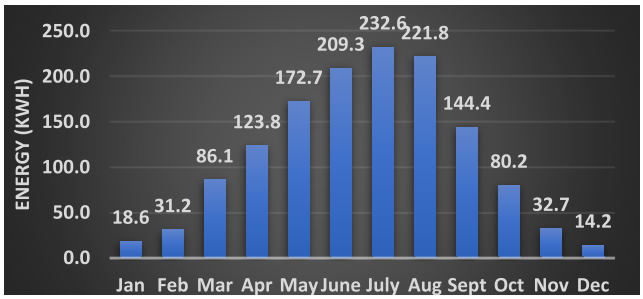

FIGURE 13. The output of one AE-21 solar thermal collector (monthly sum).

TABLE 11. Solar thermal result.

Variable	Value
Yearly Energy output (single collector)	1367.34 kWh
Daily average energy output	3.75 kWh
% of solar irradiance captured	60.97
Annual thermal load (kWh)	65805.26
No. of collectors required	48.13
Area required (m^2)	92.98
Area available (m^2)	158.95

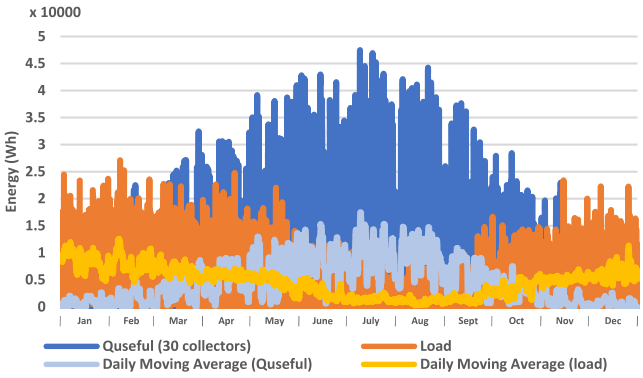

FIGURE 14. The energy output of solar collectors vs. the thermal load.

TABLE 12. Parametric sweep results.

Var.	Value							
NoC	1	5	10	15	20	25	30	48
PEE	18	33	43	50	56	61	65	74
PUL	98	93	88	84	82	80	78	74
SF	2	7	12	16	18	20	22	26
ON	1.59	1.5	1.4	1.37	1.33	1.3	1.27	1.2
PoC	0.74	3.7	7.5	11	15	18	22	35.7
ASO	14.4	14	13	12.4	12	11.7	11.5	10.9
PP	2.07	2.9	3.5	3.89	4.61	5.19	5.66	7.66
OGF	3.76	2.3	2.2	2.01	1.79	1.61	1.46	1.09
RA (%)	100%	61%	59%	54%	48%	43%	39%	29%

NoC= number of collectors, PEE= % excess energy, PUL= % of unmet load, SF= solar fraction (%), ON = Oil needed (hundred gallons), PoC= price of collectors, ASO=annual sum paid on oil (thousands), PP= payback period, OGF: oil gallons offset per 100 dollars invested, RA= relative abatement.

relative abatement. The last term is a normalization of oil gallons offset. The results are shown in Table 12 and figure 15.

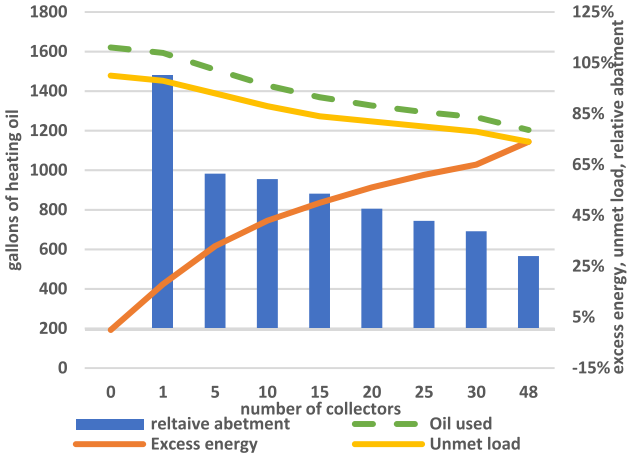

FIGURE 15. The parametric sweep of collector size results visualized.

The sweep results show that as the collector size increases, excess energy increases, and the unmet load decreases until they intersect at the point where the number of collectors is equivalent to the size of the load (i.e., 48 collectors in this case). Relative abatement, i.e., the abatement power of each 100 dollars invested, is most substantial for small collector size where excess energy is the lowest. For one collector, every 100 dollars invested can offset 3.76 gallons of oil, while for 48 collectors, they only offset 1.1 gallons. The payback period is the number of years required to make back the initial investment; the results show that as collector size increases, the payback period also increases, likely due to excess energy increasing. However, at most, the 48-collector system requires 7.7 years to recover its investment, which is acceptable.

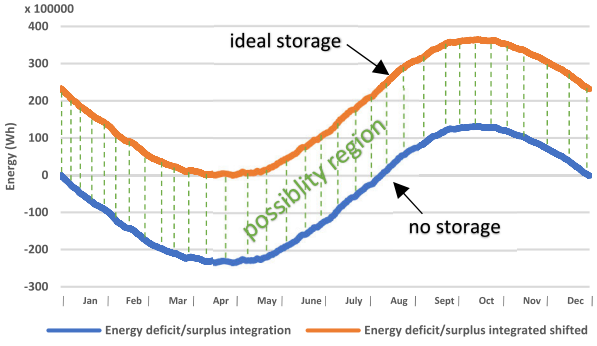

FIGURE 16. Thermal energy deficit/surplus integration showing the effect of storage on the load.

Next, the effect of storage is considered. As shown in Figure 16, the system runs at a deficit for the first quarter of the year until it reaches its lower peak in April. The deficit is gradually compensated for as the year progresses, reaching back to 0 Wh at the end of July. In the third quarter, energy surplus continues till the positive peak is reached in October, then the surplus is drained away, so the system reaches back to 0 Wh at the end of the year. Therefore, the role ideal diurnal

storage would play is shifting this curve upwards so that the lowest point the curve reaches is 0 Wh. Meaning the system would never have an overall deficit. However, to accomplish this, unrealistic storage sizes are needed. Upon inclusion of storage, the curve shifts up by some amount depending on the size of storage. The final curve will lie somewhere in the possibility region, likely closer to the no storage case due to spatial and economic constraints.

The relationship between different storage sizes and the associated solar fraction is shown in figure 17. The maximum plausible solar fraction for the system is around 50%. For this study, a 60-gallon or 227 kg storage is considered. This results in a final solar fraction of 35%, a 9% improvement over the no storage system.

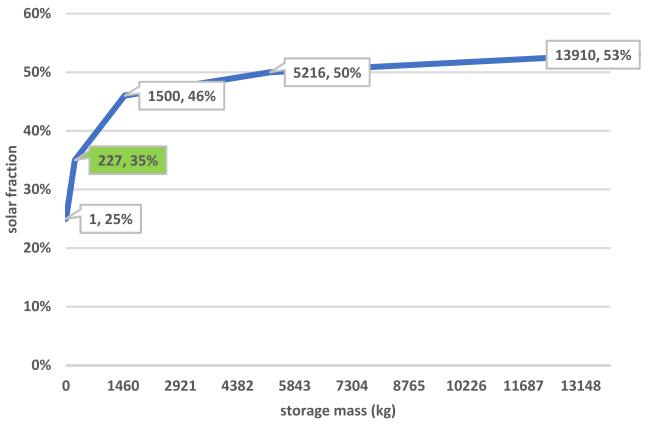

FIGURE 17. Change in solar fraction vs. change in water storage mass.

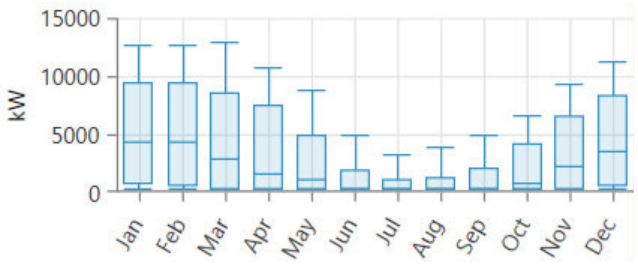

FIGURE 18. Thermal load seasonal profile for the design house.

Before installing the solar thermal system, the community's aggregate thermal load was around 22.6 GWh, while after it is around 14.9 GWh. The resulting load has a 40.7 MWh/day average energy, 1.7 MW average power, and 12.85 MW average peak with a load factor of 0.13. As can be seen from figures 18 and 19, the load peaks in January and reaches 0 kWh in some summer hours due to the solar thermal system. On the other hand, the electrical load is much more evenly distributed. The dwelling in question does not own an air conditioner (NL has much lower AC ownership than other provinces). The electric load peaks in August at 1.2 MW (6 pm is the peak hour) and otherwise has an average power load of 0.53 MW and average daily energy of 12.7 MWh/day.

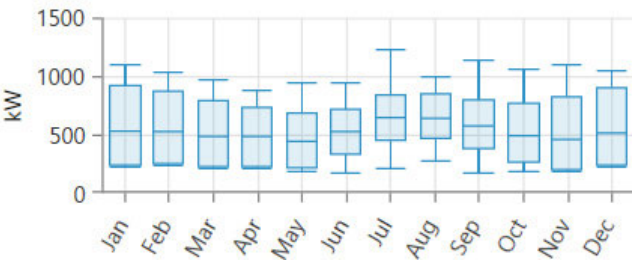

FIGURE 19. Electric load seasonal profile for the design house.

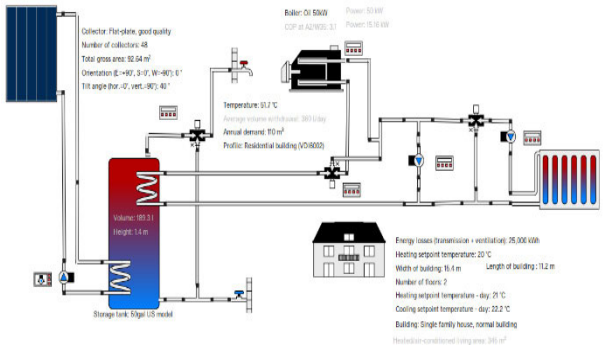

FIGURE 20. Polysun solar thermal system.

C. POLYSUN RESULTS

This section describes the actualization of the solar thermal system described earlier in the manual calculations stage. It involves the solar collector array, boiler, combi water tank, baseboard radiator, space and water loads, pumps, and the interconnection piping and controls. It was based on a built-in model that was customized and experimented with to fit the design of the proposed system. The overall system is shown in figure 20.

In the project wizard, the design house location was selected from the map (latitude of 47.5, longitude of −52.7, and elevation of 82 m). Solar thermal and boiler were selected as the energy providers, DHW and space heating as the loads (no pool heating), and "residential system" as the system size. Heat pump, Chiller, and Photovoltaics options were disabled. This narrowed down the template options from which "9u space heating and DHW" system was then selected as the system diagram most closely resembled the system envisioned during the manual calculations stage. The results as can be seen from figure 21 and Table 13 show a 34.4% solar fraction and 0.93 primary energy factor (PEF). The solar fraction is within the range provided in the methodology and close to the value obtained.

Under hot water options, 6 was selected as the number of occupants and 51.7 °C as the hot water temperature. Daily hot water demand was selected as 360 L and absences as never. Under "building", "single-family house normal building" option was selected. The length and width of the building were inputted as 11.2 m and width 15.4 m respectively (obtained from Google earth). The number of floors was set

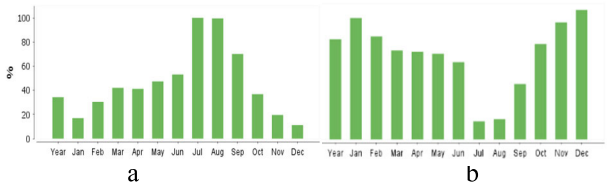

FIGURE 21. Polysun solar thermal system selected results. a) Solar fraction, b) Primary energy factor.

TABLE 13. Solar thermal polysun results.

Metric	Unit	Value
Solar fraction (total)	%	34.4
Solar fraction (hot water)	%	55.2
Solar fraction (space heating)	%	32.3
Solar thermal energy output	kWh	22,727
Total energy consumption	kWh	64,231
Primary energy factor	unitless	0.93

to two and so the heated living area then becomes 345 m (172 m per floor). The heating setpoint temperature was set to 21 °C. Under heating element, a radiator with a nominal inlet temperature of 60 °C and nominal return temperature of 21 °C were selected (assuming that, ideally, the temperature should drop to near ambient at the end of any given hour) however changing the radiator to 40 °C nominal inlet and 30 °C nominal return temperatures, yields 4% higher solar fraction and 0.14 lower primary energy factor. Low return temperatures are generally recommended for combi systems. Due to uncertainty regarding the temperature parameters of the existing radiator a conservative choice was made to keep the earlier design.

Under the Solar system, North America was selected as the test standard, AE-21 was selected as the collector module, orientation is set to 0 (south-facing) and tilt is set 40 degrees. The solar fraction was selected as "medium" from low to high options. The collector number was set as 48 which makes the gross area 92.64 m^2. Placing the storage tank outdoor (in the backyard) yields a 0.1% lower solar fraction and 0.1% higher primary energy factor.

From the load data from BEOPT, the maximum heating load that occurred at any given hour (after installing the solar thermal system) was 37.4 kW, by accounting for the 80% boiler efficiency, the boiler should have a rated power of approximately 46.75 kW so under heat generator a 50-kW boiler that uses heating oil was selected. This was close to the recommended power by Polysun. It should be noted that the boiler initially had an efficiency of 85% but was changed to 80% to match BEOPT. However, doing so had no effect on the solar fraction but it increased the primary energy factor by 0.8. The boiler has a minimum power of 10 kW and was placed indoors in a heated area (basement), not doing so reduces the solar fraction by 0.7% and increases the primary energy factor by 0.02%.

The three pumps (solar loop, boiler loop, and space heating loop) were initially selected as large with a 30% heat transfer percentage. However, changing them to small leads to the same solar fraction and primary energy factor, 0.01 kWh higher energy deficit, but an 88% (136 kWh) lower electricity consumption. Choosing a pump with 60% heat transfer such as Biral M12 for all three pumps leads to a 0.3% increase in solar fraction, no change in primary energy factor, and a 42 kWh decrease in electricity consumption over the large pumps system. Therefore, small eco pumps will be used. Pipes were given by the built-in model as 22 mm diameter copper tubes. Replacing these with the much larger 107 mm PVC pipes yielded only a 0.2% increase in solar fraction even when coupled with larger pumps. It also did not reduce stagnation time. Therefore, smaller pipes and pumps will be used.

It should be noted that Polysun is using a slightly different set of weather data (obtained from Metronome 6) than the ones used in earlier calculations and so might offer marginally different results. Losses considered by Ploysun are also more comprehensive than earlier ones. With that in mind, the difference in solar fraction between the two methods is only 0.6% which is acceptable.

D. HOMER RESULTS

The optimization's final result yields a system that utilizes solar PV, solar thermal, wind turbines, fuel cells, and hydroelectric turbine for energy generation, and hydrogen electrolysis as storage (shown in figure 22).

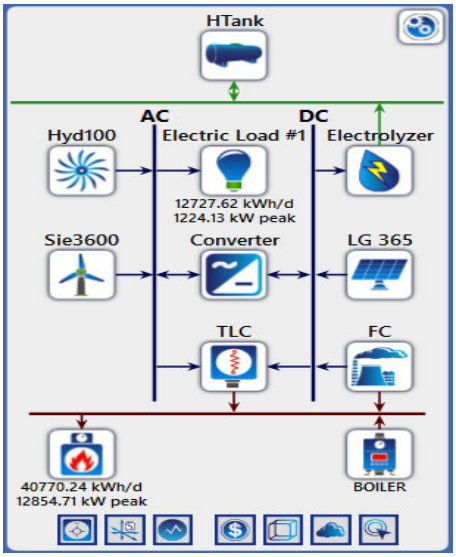

FIGURE 22. Final microgrid system schematic in HOMER including loads, generation, and storage.

The total system Net present cost is 53.7 million CAD for the 25-year project lifetime. The main cost element is the boiler's fuel cost, which consumes 986,000 L of diesel per year, which is a 71% decrease in diesel consumption as the initial load consumed 1.3 mil L of diesel for electricity

generation and 2.1 mil L for heating. The diesel consumption for electric generation is high despite the load itself being much lower than the thermal load because diesel electricity generators often have a much lower efficiency than diesel/heating oil run boilers.

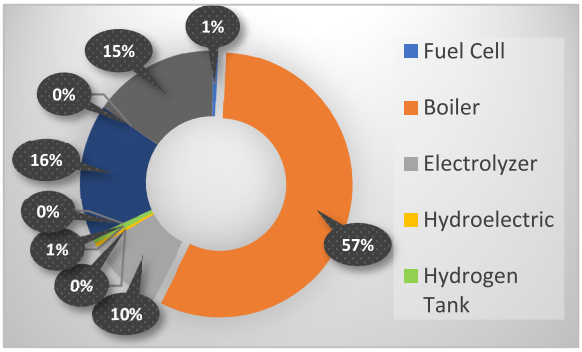

FIGURE 23. Microgrid net present cost breakdown.

Figure 23 shows the boiler fuel cost accounts for 57% of total NPC, followed by the two wind turbines' cost (16%) and the distributed solar thermal system (15%). This means fuel cost is a more considerable expense than capital cost. From the cash flow diagram, the system costs 19.2 mils in the first year in capital costs, 2.4 mils in fuel cost each year as fuel to the boiler, and 3.9 mils replacement costs in year 15 to replace some of the shorter life components which are then salvaged for 1.6 mils at the end of the project lifetime. O&M costs are minimal, accounting for only 5% of the total cost.

The size of each component and its contribution are shown in Table 14.

TABLE 14. Homer optimization results.

Comp.	No. of units	Size	Elec op	Thermal op	LCOE
WT	2	7.2 MW	21.6 GWh		0.032
PV	81	29.4 kW	35 MWh		0.091
Hydro	1	100 kW	1.1 GWh		0.017
FC	2	500 kW	60 MWh	217 MWh	
ST	344			7.7 GWh	
Boil	344			8.25 GWh	
Eh	344			6.42 GWh	
HT	1	200 kg			
El	3	990 kg			
Con	1	88 kW			

WT = wind turbine, FC = fuel cell, ST = solar thermal, HT = hydrogen tank, El = electrolyzer, con = converter, Boil = boiler, Eh = electric heater.

The majority of the electric load was served by the two wind turbines, which combined generate 94.7% of all electricity generated. Most of this electricity is more than the 4.64 MWh annual load and is labeled excess. This excess energy serves two purposes; one is that it serves the part of the thermal load that coincides with it via the electric water heater, the second purpose is that it is used to electrolyze water to produce hydrogen, which is stored in the tank for later conversion via the fuel cell system. To enumerate, 7.7 GWh (35%) of excess energy was used to serve the thermal load. In contrast, the electrolyzer uses 590.5 MWh (3.3%) to produce 12,730 kg of hydrogen per year, 99.6% of which is used by the fuel cells to produce 60.3 MWh of electricity and 217.3 MWh of thermal energy.

The system is mostly renewable with a renewable fraction of 56.4%; however, there is a sizable quantity of excess energy that needs to be dumped. One possible utilization of that energy is to expand the hydrogen system and trade the excess hydrogen with neighboring municipalities. NL has recently agreed to zero net emissions by 2050, which could mean a fundamental transformation in energy consumption that can enable a hydrogen economy.

The overall system LCOE is −0.0245 \$/kWh. To understand a negative LCOE in HOMER, we examine the LCOE equation used by the software.

$$LCOE = \frac{C_{ann,tot} - C_{boiler} * H_{served}}{E_{served}} \tag{14}$$

$$C_{boiler} = \frac{3.6(C_{fuel} + C_{boiler\ emissions})}{\eta_{boiler} * LHV_{fuel}} \tag{15}$$

where: $C_{ann,tot}$ is the total annualized cost of the system, C_{boiler} is the boiler marginal cost, H_{served} is the thermal load served, E_{served} is the electric load served, C_{fuel} = cost of fuel (\$/kg), $C_{boiler\ emissions}$ = cost penalty associated with boiler fuel (\$/kg), η_{boiler} is the boiler efficiency and LHV_{fuel} is the lower heating value of the fuel used by the boiler (M.J./kg).

From the previous equations (14 &15), we see that as the electric load's size increases, the LCOE decreases. On the other hand, the total annualized cost of the system is directly proportional to the LCOE. In electric-only microgrids, the "$C_{boiler} * H_{served}$" term is zero, and so the LCOE cannot be negative (it can only be large or small). However, in the present CHP study, the thermal load is both considered and considerable. This, accompanied by the high fuel cost, makes the negative term in the first equation bigger than the total annualized cost.

This means that money invested in the renewable system (annualized) is less than the thermal load's annual cost if the diesel system fully served the load. i.e., the LCOE turns negative when the savings due to replacing the diesel system exceed the cost of the renewable system. This LCOE would be even lower when the thermal load served by the solar thermal system is taken into account. While this result is remarkable, the cost analysis employed by HOMER is far from comprehensive. A realistic design is likely to include cost elements (such as labor and transportation costs) that can impact the results. Another limitation is that diesel's cost in this study was assumed as 2.391 \$/L based on [5]. This figure is 1 \$/L more expensive than NL's diesel price as it reflects the cost of transporting the fuel to less accessible remote locations.

VI. CONCLUSION

In conclusion, this study started by examining the 13 diesel-operated remote communities in NL based on energy consumption, population, and available renewable resources.

This resulted in the selection of Cartwright remote community for a CHP microgrid. BEOPT was used to model the load by studying a house in St. John's. Mathematical modeling was provided for solar thermal systems and used to design a distributed system which was confirmed with Polysun simulation. Location resources were obtained from a variety of sources and reported along with component selection. The effect of several solar collectors and the impact of storage on the solar fraction was reported. The final system was then obtained from HOMER, where wind turbines had the most considerable contribution to generation and diesel boiler to cost. An NPC of $53 mil for the optimal system was obtained along with a negative LCOE due to the large thermal load served.

This study combined both distributed and centralized generation and expanded the possibilities of HOMER's microgrid design by including a solar thermal system along with five other generation and storage technologies. The study also addressed the design of a CHP microgrid for a Newfoundland remote community which is seldomly addressed. The study also improved on previous studies by sizing the load using BEOPT and including hydrogen electrolysis which has economic and developmental potential. It was found that all of the electric load and most of the thermal load can be supplied by renewable sources which costed less than the diesel-only base case. The obtained results can be further generalized to other large remote communities in Canada.

REFERENCES

[1] N. Ninad, D. Turcotte, and Y. Poissant, "Analysis of PV-diesel hybrid microgrids for small Canadian arctic communities," *Can. J. Electr. Comput. Eng.*, vol. 43, no. 4, pp. 315–325, 2020, doi: 10.1109/cjece.2020.2995750.

[2] J. Tang, M. Ding, S. Lu, S. Li, J. Huang, and W. Gu, "Operational flexibility constrained intraday rolling dispatch strategy for CHP microgrid," *IEEE Access*, vol. 7, pp. 96639–96649, 2019, doi: 10.1109/access.2019.2929623.

[3] E. A. Al-Ammar, H. U. R. Habib, K. M. Kotb, S. Wang, W. Ko, M. F. Elmorshedy, and A. Waqar, "Residential community load management based on optimal design of standalone HRES with model predictive control," *IEEE Access*, vol. 8, pp. 12542–12572, 2020, doi: 10.1109/access.2020.2965250.

[4] Z. Zhou, C. Wang, and L. Ge, "Operation of stand-alone microgrids considering the load following of biomass power plants and the power curtailment control optimization of wind turbines," *IEEE Access*, vol. 7, pp. 186115–186125, 2019, doi: 10.1109/access.2019.2958678.

[5] E. G. Vera, C. Canizares, and M. Pirnia, "Renewable energy integration in Canadian remote community microgrids: The feasibility of hydrogen and gas generation," *IEEE Electrific. Mag.*, vol. 8, no. 4, pp. 36–45, Dec. 2020, doi: 10.1109/MELE.2020.3026438.

[6] I. Das and C. A. Canizares, "Renewable energy integration in diesel-based microgrids at the Canadian arctic," *Proc. IEEE*, vol. 107, no. 9, pp. 1838–1856, Sep. 2019, doi: 10.1109/jproc.2019.2932743.

[7] A. A. Eajal, A. El-Awady, E. F. El-Saadany, K. Ponnambalam, A. Al-Durra, A. Al-Sumaiti, and M. Salama, "A Bayesian approach to the reliability analysis of renewables-dominated DC microgrids," *IEEE Trans. Power Syst.*, early access, Feb. 3, 2021, doi: 10.1109/TPWRS.2021.3056314.

[8] D. Ribó-Pérez, P. Bastida-Molina, T. Gómez-Navarro, and E. Hurtado-Pérez, "Hybrid assessment for a hybrid microgrid: A novel methodology to critically analyse generation technologies for hybrid microgrids," *Renew. Energy*, vol. 157, pp. 874–887, Sep. 2020, doi: 10.1016/j.renene.2020.05.095.

[9] M. Islam, B. Das, P. Das, and M. Rahaman, "Techno-economic optimization of a zero emission energy system for a coastal community in Newfoundland, Canada," *Energy*, vol. 220, Apr. 2021, Art. no. 119709, doi: 10.1016/j.energy.2020.119709.

[10] H. Qi, H. Yue, J. Zhang, and S. Lo, "Optimal control of CHP plant integrated with load management on HVAC system in microgrid," in *Proc. IEEE 15th Int. Conf. Control Autom. (ICCA)*, Jul. 2019, pp. 1073–1078, doi: 10.1109/ICCA.2019.8899972.

[11] Z. Shen, C. Wu, L. Wang, and G. Zhang, "Real-time energy management for microgrid with EV station and CHP generation," *IEEE Trans. Netw. Sci. Eng.*, early access, Mar. 2, 2021, doi: 10.1109/TNSE.2021.3062846.

[12] E. Saloux and J. A. Candanedo, "Optimal rule-based control for the management of thermal energy storage in a Canadian solar district heating system," *Sol. Energy*, vol. 207, pp. 1191–1201, Sep. 2020, doi: 10.1016/j.solener.2020.07.046.

[13] H. Karasu and I. Dincer, "Life cycle assessment of integrated thermal energy storage systems in buildings: A case study in Canada," *Energy Buildings*, vol. 217, Jun. 2020, Art. no. 109940, doi: 10.1016/j.enbuild.2020.109940.

[14] H. Yu, K. Zhang, Y. Liu, J. Dai, and Z. Sun, "Micro-grid scheduling of electric boiler and CHP with thermal energy storage based on wind power accommodating," in *Proc. IEEE 10th Int. Symp. Power Electron. Distrib. Gener. Syst. (PEDG)*, Jun. 2019, pp. 336–340, doi: 10.1109/PEDG.2019.8807672.

[15] C. Treichel and C. A. Cruickshank, "Greenhouse gas emissions analysis of heat pump water heaters coupled with air-based solar thermal collectors in Canada and the United States," *Energy Buildings*, vol. 231, Jan. 2021, Art. no. 110594, doi: 10.1016/j.enbuild.2020.110594.

[16] M. Mansoor, M. Stadler, H. Auer, and M. Zellinger, "Advanced optimal planning for microgrid technologies including hydrogen and mobility at a real microgrid testbed," *Int. J. Hydrogen Energy*, vol. 46, no. 37, pp. 19285–19302, May 2021, doi: 10.1016/j.ijhydene.2021.03.110.

[17] J. Pascual, D. Arcos-Aviles, A. Ursúa, P. Sanchis, and L. Marroyo, "Energy management for an electro-thermal renewable–based residential microgrid with energy balance forecasting and demand side management," *Appl. Energy*, vol. 295, Aug. 2021, Art. no. 117062, doi: 10.1016/j.apenergy.2021.117062.

[18] C. A. Díaz González and L. Pacheco Sandoval, "Sustainability aspects of biomass gasification systems for small power generation," *Renew. Sustain. Energy Rev.*, vol. 134, Dec. 2020, Art. no. 110180, doi: 10.1016/j.rser.2020.110180.

[19] B. Li and J. Li, "Sizing versus price: How they influence the energy exchange among large numbers of hydrogen-centric multi-energy supply grid-connected microgrids," *Energy Rep.*, vol. 6, pp. 1557–1567, Dec. 2020, doi: 10.1016/j.egyr.2020.10.052.

[20] S. Motahar and H. Bagheri-Esfeh, "Artificial neural network based assessment of grid-connected photovoltaic thermal systems in heating dominated regions of Iran," *Sustain. Energy Technol. Assessments*, vol. 39, Jun. 2020, Art. no. 100694, doi: 10.1016/j.seta.2020.100694.

[21] C. Artur, D. Neves, B. C. Cuamba, and A. J. Leão, "Comparison of two dynamic approaches to modelling solar thermal systems for domestic hot water," *Sustain. Energy Technol. Assessments*, vol. 30, pp. 292–303, Dec. 2018, doi: 10.1016/j.seta.2018.10.012.

[22] A. Guerello, S. Page, G. Holburn, and M. Balzarova, "Energy for off-grid homes: Reducing costs through joint hybrid system and energy efficiency optimization," *Energy Buildings*, vol. 207, Jan. 2020, Art. no. 109478, doi: 10.1016/j.enbuild.2019.109478.

[23] M. Wei, S. H. Lee, T. Hong, B. Conlon, L. McKenzie, B. Hendron, and A. German, "Approaches to cost-effective near-net zero energy new homes with time-of-use value of energy and battery storage," *Adv. Appl. Energy*, vol. 2, May 2021, Art. no. 100018, doi: 10.1016/j.adapen.2021.100018.

[24] A. Allouhi, S. Rehman, and M. Krarti, "Role of energy efficiency measures and hybrid PV/biomass power generation in designing 100% electric rural houses: A case study in Morocco," *Energy Buildings*, vol. 236, Apr. 2021, Art. no. 110770, doi: 10.1016/j.enbuild.2021.110770.

[25] R. Neves, H. Cho, and J. Zhang, "Pairing geothermal technology and solar photovoltaics for net-zero energy homes," *Renew. Sustain. Energy Rev.*, vol. 140, Apr. 2021, Art. no. 110749, doi: 10.1016/j.rser.2021.110749.

[26] B. Hodge, *Alternative Energy Systems and Applications*, 2nd ed. Hoboken, NJ, USA: Wiley, 2017, pp. 143–167.

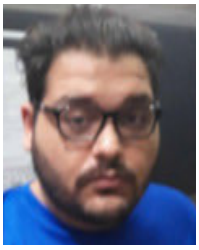

HASHEM ELSARAF (Graduate Student Member, IEEE) was born in Alexandria, Egypt, in 1992. He received the B.Sc. degree in electronics and communications engineering from the Arab Academy for Science and Technology, Alexandria, in 2017, and the M.Sc. degree in energy from Heriot-Watt University, Edinburgh, U.K., in 2018. He is currently pursuing the M.A.Sc. degree in energy systems engineering with Memorial University, NL, Canada. His thesis involved the design of a 3-D printed vibration energy harvester for ultra-low-power sensors applications. He is the winner of the first-class in program scholarship for M.A.Sc. Energy Program.

MOHSIN JAMIL received the Ph.D. degree in electrical engineering from the University of Southampton, U.K., in 2012. From 2012 to 2016, he worked at the Robotics Department, National University of Sciences and Technology (NUST), Islamabad, Pakistan. From 2016 to 2019, he worked at the Department of Electrical Engineering, Islamic University of Madinah, Saudi Arabia. He is currently a Faculty Member of the Department of Electrical Engineering, Memorial University. He is the author or coauthor of several IEEE publications in different journals and peer-reviewed conferences. He was a recipient of different awards and funding grants. He is an Associate Editor of IEEE Access.

BISHWAJEET PANDEY (Senior Member, IEEE) received the M.Tech. degree in computer science engineering (CSE) from IIIT Gwalior, with specialization in VLSI, the M.C.A. degree in research and development project from CDAC, Noida, and the Ph.D. degree in computer science engineering (CSE) from Gran Sasso Science Institute, L'Aquila, Italy, under guidance of Prof. Paolo Prinetto, Politecnico Di Torino (World Ranking 13 in Electrical Engineering). He has worked as an Assistant Professor with the Department of Research, Chitkara University, India; as a Junior Research Fellow (JRF) at South Asian University, India; as a Lecturer at Indira Gandhi National Open University, India; and as a Visiting Lecturer at Aalborg University, Denmark. He is currently working as an Assistant Professor at the Birla Institute of Applied Sciences, Bhimtal, India, and also working as an Adjunct Professor at UCSI University, Malaysia. He has authored or coauthored more than 200 articles.